ORIGINAL RESEARCH ARTICLE

In Situ Monitoring of Retained Austenite Decomposition During Tempering of High-Strength Tool Steels

MYRIAM DUMONT, MAHA MESSAADI BEN SAID, MARINE LACHAL, DAVID QUIDORT, MAXIME PERRUCHOT, BENOÎT MALARD, NORBERT SCHELL, EMAD MAAWAD, DENIS DELAGNES, and MOUKRANE DEHMAS

This study investigates the decomposition of retained austenite (RA) in tool steels for plastic molding in correlation with the alloy chemical composition and the tempering parameters. Two grades differing in their silicon content with initial mixed bainitic/martensitic microstructures were investigated using *in situ* synchrotron high-energy X-ray diffraction (HEXRD) during tempering in the 550 °C to 600 °C temperature range for one-hour holding time. Results indicated carbide formation during heating or isothermal holding; however, retained austenite remained untransformed up to the end of the tempering holding time in all investigated conditions for both grades. *In situ* HEXRD provides direct evidence of the transformation of retained austenite into fresh martensite on cooling from the tempering stage. This behavior is correlated to the evolution of carbon enrichment of retained austenite and the effect of silicon is discussed.

https://doi.org/10.1007/s11661-025-07847-9

I. INTRODUCTION

PLASTIC injection molding requires the use of molds inserts and holders made of high-strength steel capable of withstanding cyclic high stresses resulting from high injection pressures. High hardness and mechanical properties are required for durability (wear and fatigue resistance), while good machinability, optimal surface finish after polishing, and good thermal conductivity to remove heat dissipated during cooling of the molded parts are equally important.

Today mold parts are preferably machined directly from a high-quality prehardened steel block of high mechanical properties obtained by a controlled quenching and tempering process. While it is nowadays possible to machine hard materials over a wide range of cutting speeds, available prehardened grades generally present hardness levels ranging from 30 to 40 HRC. To achieve higher properties, mold makers are increasingly using ASTM A681 H11 or H13 grades, which are machined in the annealed condition and require final heat treatment of the parts to reach the desired hardness. However, those steels were designed many decades ago for hot working processes such as forging, or high pressure die casting where they are exposed to severe working conditions with rapid changes in temperature up to 600 °C and high mechanical loads.[1] However, the requirements for use as components in plastic injection molds are lower than for hot working. Furthermore, the high chromium content in H11 or H13 impairs the thermal conductivity for those grades, which is a key characteristic for plastic molding applications.[2] Consequently, new developments focus on the production of a new grade with reduced contents of Cr, Mo, and V, and having a typical hardness in the delivery condition of 44 HRC (1400 MPa UTS) with excellent machinability.

From the perspective of steel manufacturers, the thickness of prehardened steel blocks has increased with the demand for ever larger parts, leading to large

MYRIAM DUMONT, MAHA MESSAADI BEN SAID, and MAXIME PERRUCHOT are with the MSMP-EA7350, Arts et Métiers Institute of Technology, 8 Bd de Louis XIV, 59000 Lille, France. Contact e-mail: myriam.dumont@ensam.eu MARINE LACHAL and DAVID QUIDORT are with the Industeel, ArcelorMittal Group, 71200 Le Creusot, France. BENOÎT MALARD and MOUKRANE DEHMAS are with the CIRIMAT, Université Toulouse, CNRS, 4 allée Emile Monso BP44362, 31030 Toulouse Cedex 4, France. NORBERT SCHELL and EMAD MAAWAD are with the Institute of Materials Physics, Helmholtz-Zentrum Hereon, Max-Planck-Straé 1, 21502 Geesthacht, Germany. DENIS DELAGNES is with the Institut Clént Ader ICA; Université de Toulouse; CNRS, IMT Mines Albi, INSA, ISAE- SUPAER, UPS Campus Jarlard, 81013 Albi France
Manuscript submitted December 4, 2024; accepted May 26, 2025.

Published online: 19 June 2025

temperature gradients during the quenching process. As a result, the as-quenched microstructure can vary from fully martensitic microstructure to variable proportions of bainite and retained austenite as a function of depth.[3,4] The evolution of this latter phase during tempering is of prime importance, when dealing with the final properties. In most cases depending on alloy composition and parameters of the heat treatments, retained austenite is expected to decompose into ferrite and carbides during tempering.[5,6] Some authors observed different behaviors, such as the transformation into bainite[7–9] or no decomposition during the tempering stage itself followed by a transformation into fresh martensite on final cooling.[10–12] Moreover, the addition of some alloying elements like silicon or aluminum is known to prevent precipitation of iron carbides during the bainitic transformation; this is expected to modify the carbon enrichment of the retained austenite and thus its stability and decomposition sequence. Even if many publications deal with the decomposition kinetics of retained austenite during tempering in steels with as-quenched martensitic microstructures, less data are available on the evolution of initial bainitic or mixed bainite/martensite microstructures.[10,13,14] In many cases, the understanding of phenomena is inferred from measurements of post-mortem microstructural features and/or relevant physical properties such as dilatometry,[15] magnetic and electrical resistivity[16] , and *in situ* high-energy X-ray diffraction (HEXRD). The advantages of *in situ* HEXRD, such as high penetration depth and acquisition time that can be drastically reduced to one-tenth of a second, enable monitoring the kinetics of rapid phase transformation. Up to now, literature mainly provides information on the martensite evolution during tempering at the heating rates close to the equilibrium condition.[17–19] However, it is worth mentioning the work of Ribamar *et al.*[20] by HEXRD, which demonstrated the relevance of heating rate to the competition between carbon partitioning and retained austenite decomposition in the case of high-carbon high-silicon steel. Additionally, *in situ* HEXRD was preferred to prove that the austenite can be retained by the strains induced by martensite formation.[21] Unfortunately, all these findings are not sufficient to predict retained austenite decomposition kinetics under rapid heating during tempering considering different initial microstructures.

These considerations prompted this work that is focused on the study of the decomposition of retained austenite in the frame of the development of new steel grades for molding injection with initial bainitic/martensitic microstructure. The influence of the tempering parameters is investigated on two steel grades having identical chemical composition unless the silicon amount, by means of *in situ* synchrotron HEXRD, accompanied by metallographic observations.

II. EXPERIMENTAL DETAILS

A. *Samples Preparation*

Two low-carbon steels were lab-cast and processed by ArcelorMittal, Industeel. Table I displays the chemical composition of the two alloys; the two grades differ in their Si content (low Si for A grade and high Si for B grade), all other elements were kept identical. Figure 1 displays the heat treatment used for both steels.

The austenitization treatment at 1100 °C, followed by a rapid cooling from 1100 °C to 900 °C and a slow cooling at 0.028 °C/s from 900 °C to room temperature, was performed by ArcelorMittal, Industeel. The measured samples have cylindrical geometry about 6 mm in diameter and 10 mm in length, prepared by precision machining. *In situ* HEXRD experiments were performed to investigate the subsequent tempering (see Section II–B). The influence of tempering temperature was evaluated considering three different temperatures: 550 °C, 575 °C, and 600 °C. In this study, we also report the results of the influence of heating rate on tempering behavior. Two rates were investigated: a low heating within $X = 1$ °C/s and rapid heating within $X = 100$ °C/s.

B. *In Situ Synchrotron HEXRD*

HEXRD experiments offer the opportunity to perform *in situ* measurements to study the complex phase transformations during thermal treatments.[22–25] Experimentations were conducted at the Deutsches Elektronen Synchrotron (DESY) in Hamburg, Germany, on Petra III P07B beamline. A more detailed description of the HEXRD experiment is provided in.[24,26] Both steels were analyzed in transmission mode with a monochromatic beam of 87 keV ($\lambda = 0.14235$ Å). As the second harmonic with low flux density was not filtered by the optics, low-intensity peaks appeared at angles approximately half those of the main high-intensity peaks. It should be noted that the second harmonic was considered in the Rietveld refinements.

To study the tempering process, the as-received samples were heated at two different rates: a slow rate of 1 °C/s and a fast rate of 100 °C/s. Heating started from room temperature and continued up to one of three tempering temperatures (550 °C, 575 °C, or 600 °C), followed by a 1-hour holding period at the target temperature, and then cooling at 2.5 °C/s. Debye–Scherrer diffraction patterns were continuously recorded throughout the tempering cycle, using either a fast acquisition time (0.1 second) or a slow one (5 seconds), depending on the heating rate. The slow acquisition mode was used during the isothermal holding and cooling stages.

The recorded diffraction patterns were integrated to generate one-dimensional (1D) diffractograms using the Fit2D software,[27] with a standard LaB_6 powder used for calibration. The major phases were first analyzed using the Rietveld refinement method implemented in FullProf software.[28] Two distinct crystal structures were identified:

Table I. Nominal Chemical Composition (Wt Pct) of Studied Steels

Steel	C Wt Pct	Mn Wt Pct	Si Wt Pct	Cr Wt Pct	Mo Wt Pct	Ni Wt Pct	Al Wt Pct	V Wt Pct	N Wt Pct
A	0.35	0.9	0.14	2.0	0.8	0.8	0.05	0.3	0.004
B	0.35	0.9	0.57	2.0	0.8	0.7	0.05	0.3	0.004

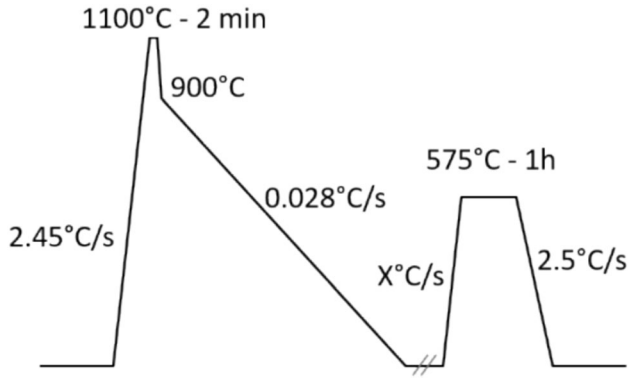

Fig. 1—Schematic diagram of conventional heat treatments.

- a body-centered cubic (bcc) phase, corresponding to the α-ferritic structure, which may include α-ferrite, bainitic ferrite, or martensite;
- a face-centered cubic (fcc) phase, with lattice parameters matching those of the γ-phase, associated with retained austenite.

The analysis gives the mass fraction of each phase and their mean lattice parameter. An error calculated as three times the standard deviation provided by the software is used to estimate the accuracy of the mass fractions. The error is found to be about 0.3 pct for austenite mass fraction.

In a second step, low-intensity peaks' characteristics of minor phase components were investigated to identify the nature of the precipitates and quantify their mass fraction.

C. *Metallographic Investigation*

For the optical and scanning electron microscopy (SEM) metallographic study, small samples were cut from the as-received or tempered samples perpendicular to the longitudinal axis of cylinders. Samples for microstructural observation were grinded by using SiC papers in the order of 500, 800, 1200, and 4000 grit and then polished with 3 and 1 μm diamond solution. For microstructural observations, the samples were immersed in 3 pct Nital reagent for a few seconds immediately after the polishing steps. To evidence retained austenite, chemical etching was performed using Behara's solution for reaction times of 3.5 minutes. A digital microscope (Keyence VHX-7000N) and a TESCAN MIRA2 SEM microscope in secondary electrons mode were used to characterize the microstructure.

Transmission electron microscopy was performed on carbon replica with a JEOL 2100F equipped with EDS for chemical analysis and mapping and ASTAR system for crystallographic determination from diffraction patterns.[29] Only grade A in its initial state and as-tempered was characterized by TEM.

III. RESULTS

A. *Initial Microstructures*

The initial microstructures after austenitizing and cooling for grades A and B are displayed in Figure 2. Etching of grade A [Figure 2(a)] reveals alternating white and dark regions, commonly referred as a banded structure. This feature is generally attributed in the literature to the microsegregation of substitutional elements occurring during casting and subsequent solid-state transformations, leading to chemical banding.[30] For the Si-rich alloy (grade B), this banded structure is not observed; however, it might be due to etching conditions. In terms of microstructure, in both grades, a typical bainitic structure can be identified with some white regions typical of martensite/retained austenite. Retained austenite mainly appears as M/A blocks. Some austenitic films can be observed, mainly in grade B. However, from such observations, it is difficult to quantify the fraction of retained austenite as a function of its morphology. The Vickers hardness (1 kgF) measured for grades A and B in their initial state is 430 ± 10 and 405 ± 10 HV, respectively. This value range is typical for bainitic microstructures.

Before any *in situ* tempering experiment, as-received samples were carefully studied by HEXRD. Typical XRD patterns are displayed in Figure 3 for both steels. As expected, all major peaks are identified as austenite (γ) or ferrite (α). Austenite peaks confirm the presence of retained austenite in the initial states in both steels. Its mass fraction was evaluated to 12 ± 0.5 pct in grade A and 26 ± 1 pct in grade B. Figure 3(b) is added to highlight the presence of minor phases. It states that the two grades have different initial states in terms of minor components. As illustrated in the Figure 3(b), the grade A presents low-intensity peaks especially at low angles. To identify these peaks, their positions were compared with reference patterns of various carbides, including chromium and iron carbides. Ultimately, all peaks were indexed as cementite, M_3C (also known as θ-carbide). Such micrometer-sized precipitates were also observed by transmission electron microscopy (TEM) carried out on grade A in its initial state (see Figure 4) and identified as cementite using ASTAR diffraction pattern

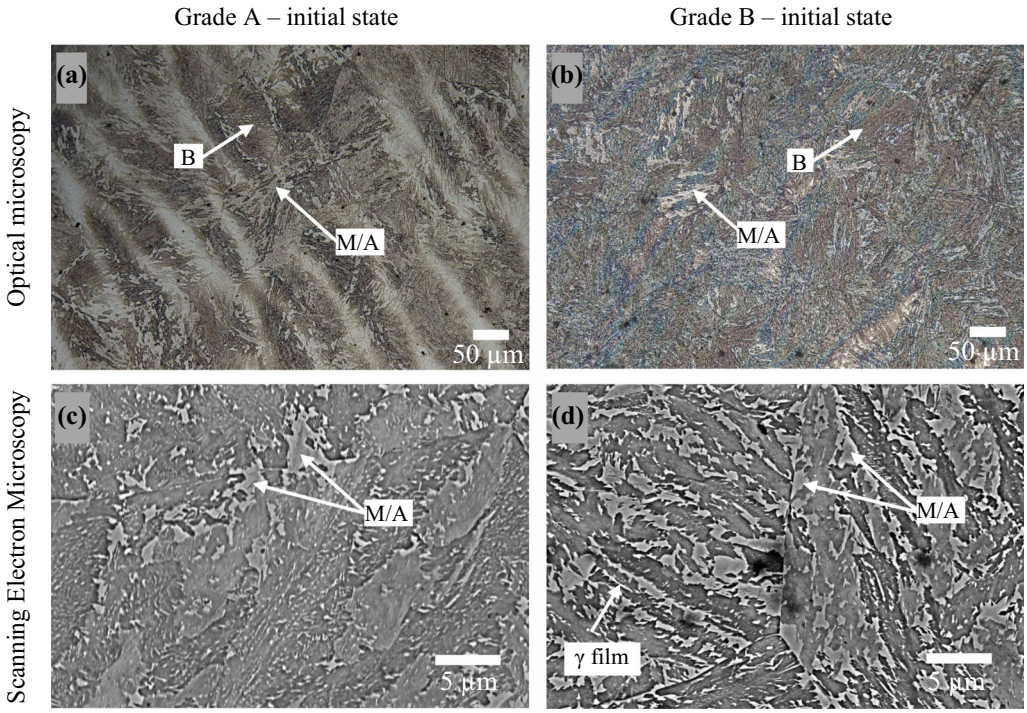

Fig. 2—Microscopic observations by optical microscopy (*a*) and (*b*) and SEM (*c*) and (*d*) of steel grades A and B in their initial state; (a) and (c) microstructure of grade A, (b) and (d) microstructure of grade B (B means bainitic region, M/A means martensite/retained austenite regions and γ film means austenitic film).

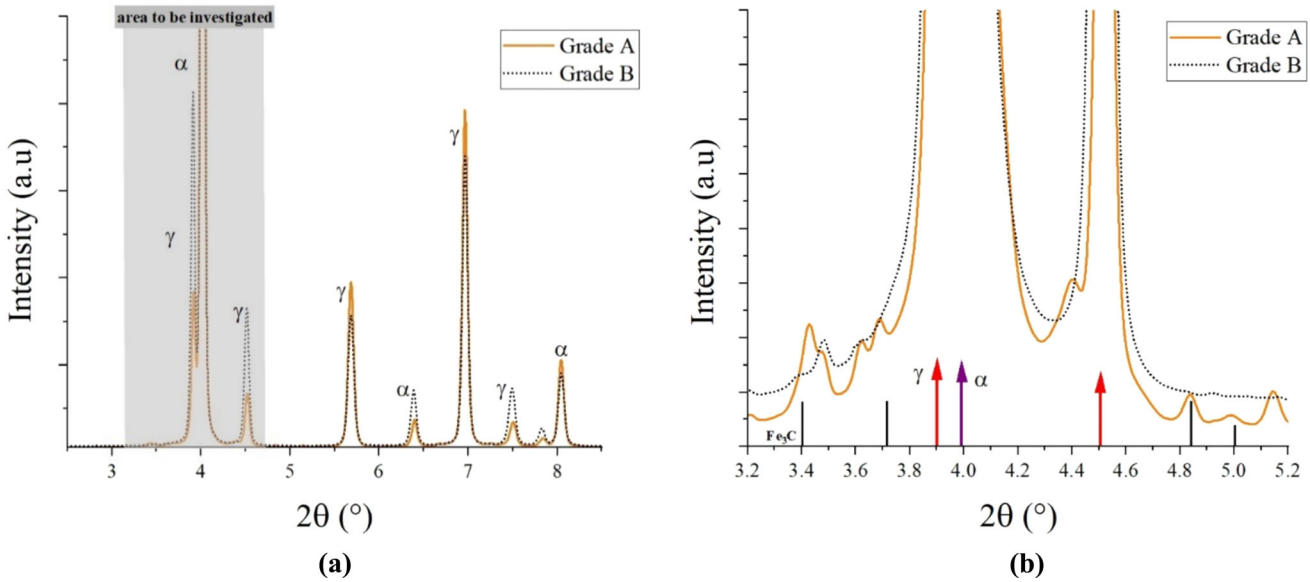

Fig. 3—X-ray diffraction data from grade A and B in their initial state; (*a*) whole window of the XRD patterns, (*b*) zoom in investigated area of XRD patterns.

identification and chemical analysis [cementite in red color in Figure 4(b)]. Some smaller co-precipitates identified by ASTAR method as AlN [in blue in Figure 4(b)] and V(C,N) [in yellow in Figure 4(b)] were also observed by TEM. These latter ones are too small and not numerous enough to be detected by HEXRD. It should be noted that no transition ε-carbides were detected. In the following, the term carbides will be used to identify the phase corresponding to the extra-diffraction peaks. In the case of the grade B, the XRD pattern does not exhibit the presence of carbide peaks. Finally, grade A consists mainly of bainitic ferrite/martensite with 12 pct retained austenite and a low amount of carbides, of the order of 1 pct as estimated by Rietveld analysis, whereas the Si-rich grade B has a higher retained austenite amount, 26 pct, and a very small

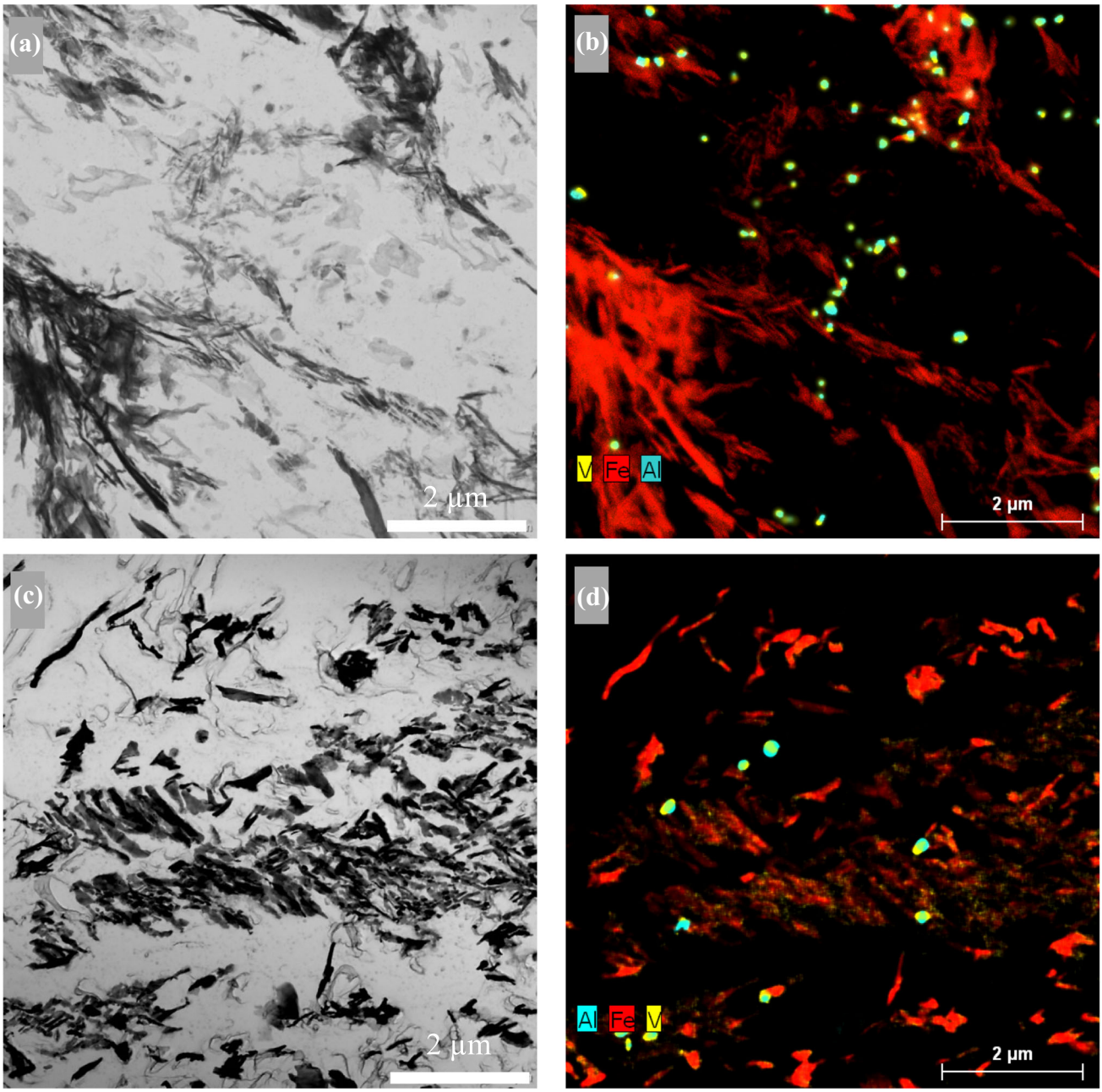

Fig. 4—TEM observations on carbon replica of grade A in its initial state (*a*) and (*b*) and after tempering for 1 hour at 575 °C (*c*) and (*d*); (a) and (c) bright field images, (b) and (d) EDS mapping showing particles enriched in vanadium (yellow), iron (red), and aluminum (blue) (Color figure online).

amount of carbides estimated to be less than 1 pct by Rietveld analysis.

B. *Decomposition of Retained Austenite During Tempering*

Figure 5(a) describes the quantitative evolution of the retained austenite as a function of temperature for a tempering at 575 °C for one hour using the heating rate 1 °C/s for both grades. Each curve highlighted in Figure 5(a) corresponds to the three phases of tempering process; the heating, the holding time during tempering at 575 °C, and the cooling. Moreover, Figure 5(b) shows the influence of the heating rate on the retained austenite mass fraction variation across the tempering process phases.

As previously reported in other studies,[6] decomposition begins during heating, marked by a slight decrease in the amount of retained austenite around 300 °C, typically attributed to carbide formation. The transformation continues during tempering at 575 °C, but to a limited extent: The retained austenite content decreases to 10 pct in grade A (from 12 pct initially) and to 24 pct in grade B (from 26 pct) after one hour of holding. This

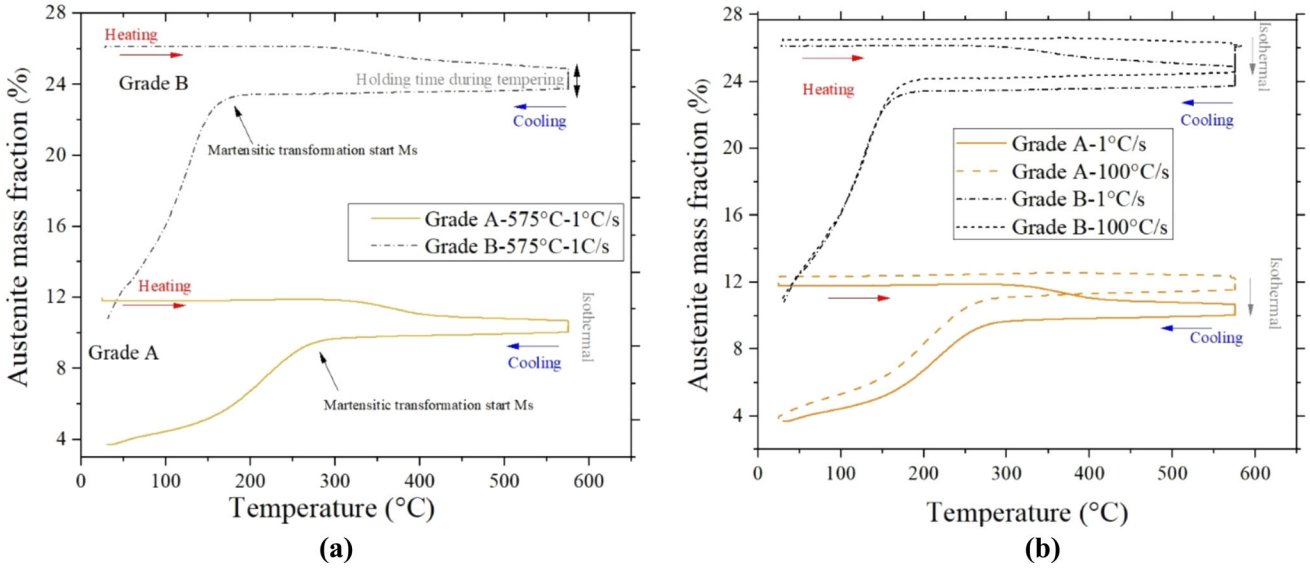

Fig. 5—Comparison of the evolution of the retained austenite mass fractions measured by HEXRD of both grades A and B; (*a*) evolution of the retained austenite mass fraction as a function of temperature at a heating rate of 1 °C/s, (*b*) influence of the heating rate on the retained austenite mass fraction variation as a function of temperature.

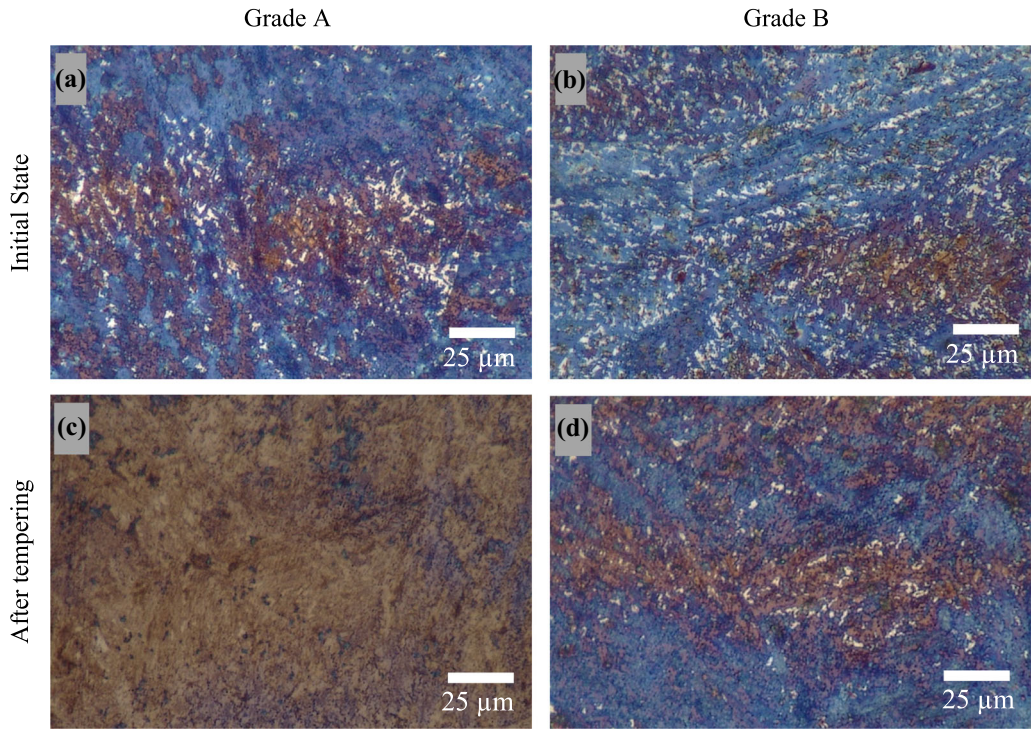

Fig. 6—Microstructural observations by optical microscopy after Behara's etching (in white: retained austenite; in color: other phases) of grade A—(*a*) and (*c*) and B—(*b*) and (*d*) in the initial state—(a) and (b) and after tempering at 575 °C for 1 h—(c) and (d).

indicates that a significant fraction of retained austenite remains untransformed after the heating and tempering stages. During final cooling, this remaining austenite transforms into fresh martensite, as shown in Figure 5. At room temperature, most of the retained austenite in grade A has decomposed, with a final content estimated at 3 pct. In contrast, grade B retains a larger fraction, estimated at 11 pct. Figure 6 presents the microstructures of grades A and B at the end of the tempering cycle (1 °C/s heating rate, 1 h holding at 575 °C), after etching with Behara's solution, which highlights retained austenite in white. These micrographs support the HEXRD findings, confirming the significant difference in retained austenite content between the two

grades: near-complete decomposition in grade A and a substantially higher retained fraction in grade B.

TEM observations of grade A after tempering [Figures 4(c) and (d)] do not show any significant changes in the precipitation state. The identified precipitates are the same as those observed prior to tempering, namely, cementite and co-precipitates of AlN and V(C,N). Such precipitates have already been observed after tempering in similar steels.[31–33] A potential increase in the volume fraction of these precipitates cannot be confirmed using carbon replica imaging alone.

C. *Influence of the Tempering Heating Rate on the Decomposition of Retained Austenite*

Figure 5(b) describes the quantitative evolution of the retained austenite as a function of temperature for a tempering at 575 °C for one hour, using two heating rates (1 and 100 °C/s) for both grades. During the heating stage, the decomposition of retained austenite is influenced by the heating rate in a similar manner for both grades. Under rapid heating (100 °C/s), the retained austenite content remains nearly constant up to the tempering temperature. In contrast, with slow heating (1 °C/s), decomposition begins around 300 °C for both grades. This early-stage transformation is reflected by a gradual decrease in retained austenite content, with similar reductions observed in both grades (− 1.2 pct for grade A and − 1.3 pct for grade B compared to their initial values).

As a result, both grades begin the tempering holding stage with a retained austenite content nearly equal to the initial value under fast heating conditions, and with a lower content under slow heating (see Table II). Furthermore, the holding stage promotes additional decomposition of retained austenite, as indicated by the vertical lines in Figure 5. In Figure 5(b), it is evident that the two grades exhibit different behaviors during this stage. For the silicon-rich steel (grade B), the decrease in retained austenite content during holding is more pronounced: approximately − 1.4 pct for the fast heating rate and − 1.2 pct for the slow rate. In contrast, for grade A, the extent of decomposition is less sensitive to the heating rate, with reductions of − 0.8 and − 0.7 pct for the fast and slow rates, respectively. At the end of the tempering holding stage, the samples subjected to slow heating contain the lowest amount of retained austenite.

As shown in Figure 4, the cooling stage can be divided into two regions: before and after the martensite start (M_s) temperature. Between the tempering temperature and Ms, the retained austenite content remains nearly unchanged. Upon reaching Ms, it decreases rapidly, indicating the onset of the martensitic transformation. Notably, the Ms temperature is independent of the heating rate but differs significantly between the two grades. It was estimated at 300 °C for grade A and 175 °C for grade B, highlighting the strong influence of silicon content on Ms. The final stage of retained austenite decomposition appears to be largely unaffected by the heating rate, with both fast- and slow-heated samples exhibiting similar retained austenite contents at room temperature: 3 pct for grade A and 11 pct for grade B.

The evolution of the minor phases during the tempering heat treatment is described in Figures 7(a) and (b) (grade A) and 7(c) and (d) (grade B) for both grades and the two heating rates. In each figure, fours patterns at key times are gathered:

- the heating start (HS) corresponds to the initial pattern similar to the as-received samples presented in Figure 3(b),
- the end of the heating (EH) corresponds to the pattern at 575 °C at the beginning of the tempering stage,
- the end of the tempering holding time (ES) corresponds to the pattern after 1 h at 575 °C and before the start of the cooling stage,
- the end of the cooling (EC) is the pattern at room temperature corresponding to the end of the tempering process.

With regard to XRD patterns collected for the grade A with slow heating rate [see Figure 7(a)], the main change consists in the reinforcement of the cementite peaks with relative increase in intensity. No structural changes are visible during holding stage and cooling except a slight continuous increase in cementite peak intensity. Then, the retained austenite decomposition that starts during the heating stage is correlated to the development of carbides. Nonetheless, for fast heating rate [see Figure 7(b)], the carbide precipitation occurs mainly during the holding stage.

In the case of the Si-rich grade B [see Figures 7(c) and (d)], it appears that the heating rate has no effect on the steel structure: In both cases, carbide cementite peaks

Table II. Evolution of Retained Austenite Amount (pct m) at the Different Tempering Stages

	Initial State	End of Heating	End of Tempering Holding Time	End of Cooling
A-575 °C-1	12.0	10.5	10.0	3.0
A-575 °C-100	12.5	12.5	11.5	4.0
B-575 °C-1	26.0	25.0	23.5	11.0
B-575 °C-100	26.5	26.0	24.5	11.0

Values are given with an error of ± 0.3 pct m estimated as three times the standard deviation given by the Fullprof software.

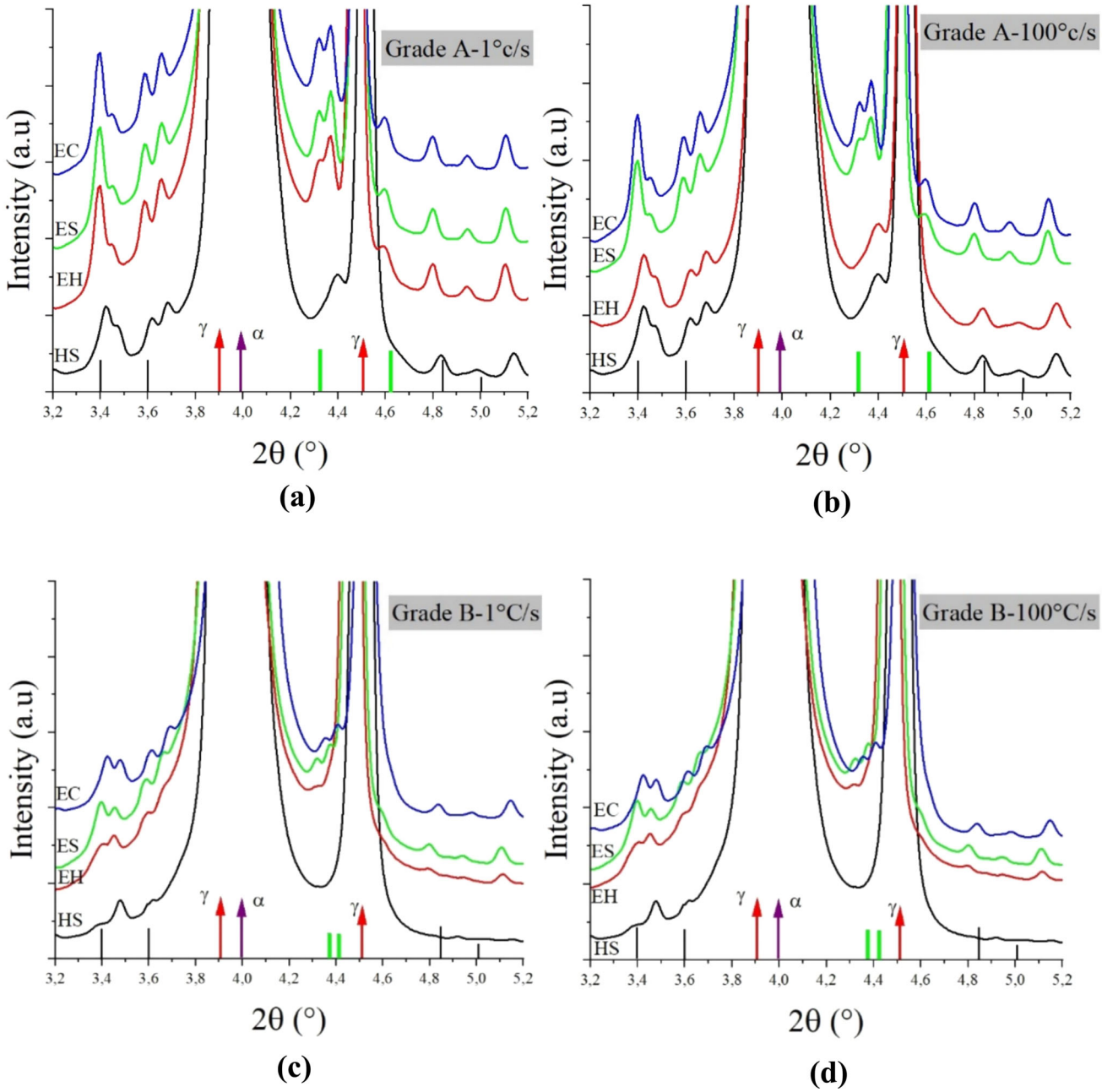

Fig. 7—*In situ* HEXRD patterns during tempering process as a function of heating rates; (*a*) grade A at 1 °C/s, (*b*) grade A at 100 °C/s, (*c*) grade B at 1 °C/s, (*d*) grade B at 100 °C/s (*HS* heating start, *EH* end of heating, *ES* end of soaking, *EC* end of cooling).

can be observed with equivalent intensities. Meanwhile, carbide peaks are present at the end of the holding stage meaning that their growth occurs at high temperature. At the end of the tempering process, decomposition of retained austenite results in fresh martensite, retained austenite, and carbides. Fast heating rate allows to inhibit the decomposition of retained austenite during heating, but it partially decomposes during holding time at 575 °C by promoting formation of carbides. However, the slow rates give the time to retained austenite to transform progressively during heating promoting the development of carbides as widely reported in literature.[24,25,24–25]

D. *Evolution of Mean Lattice Parameter of Retained Austenite and Bainitic Ferrite*

Figure 8 compares the mean lattice parameters of ferrite (including bainitic ferrite and martensite) and retained austenite during tempering, as a function of temperature, for both heating rates. Typically, the linear increase or decrease in lattice parameter during heating or cooling is attributed to thermal expansion or contraction. Under slow heating, slight deviations from linearity are observed in grades A and B [Figure 8(a)]. The magnitude of the drop during the isothermal holding period appears to differ between the two grades, suggesting a variation in the chemical composition of

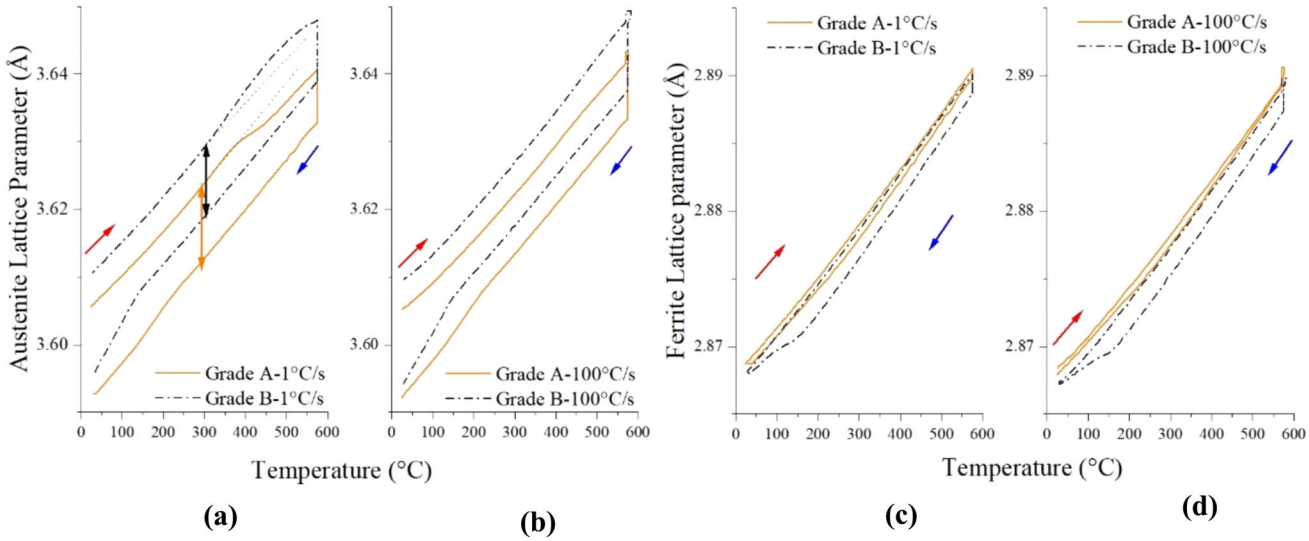

Fig. 8—Mean lattice parameter evolution during the tempering process of grades A and B; (*a*) retained austenite lattice parameter variation at a heating rate of 1 °C/s, (*b*) retained austenite lattice parameter variation at a heating rate of 100 °C/s, (*c*) martensite/ferrite lattice parameter variation at a heating rate of 1 °C/s, (*d*) martensite/ferrite lattice parameter variation at a heating rate of 100 °C/s. The arrows on figure (a) illustrate the variation in lattice parameter at 300 °C considered to evaluate the carbon content variation in retained austenite during tempering.

retained austenite. This aspect is further discussed in Section IV–B. In addition, the lattice parameter of ferrite in grade A remains nearly constant, in contrast to the evolution observed in grade B, which reflects changes in carbon enrichment of the ferrite phase regardless of the cooling temperature [Figures 8(c) and (d)].

E. *Influence of the Tempering Temperature on the Decomposition of Retained Austenite*

Since the heating rate was shown to have minimal influence on the final retained austenite content, the following analysis focuses on the effect of tempering temperature, using a fixed heating rate of 1 °C/s. Figure 9 displays the evolution of the amount of retained austenite during the tempering process for both grades A and B. During the heating and holding stages, the evolution of retained austenite content is very similar across all tempering temperatures, and the transformation kinetics appear unaffected by the selected temperature. In contrast, the cooling stage reveals clear differences in the transformation of retained austenite into martensite for both alloys. Notably, the martensite start (Ms) temperature shifts upward by approximately 50 °C when the tempering temperature is increased to 600 °C, and downward when it is reduced to 550 °C. This behavior indicates that the stability of retained austenite increases as the tempering temperature decreases.

The stability of retained austenite is highly correlated with its carbon content. As the lattice parameter is also dependent on the carbon content of the phase, the evolution of the relative lattice parameter during tempering holding stage is considered. Figure 10 illustrates the variation of the normalized lattice parameter of retained austenite as a function of tempering holding time and temperature. The relative lattice parameter was obtained by normalizing the measured values to those at the beginning of the holding period, in order to eliminate the influence of thermal expansion, including any contribution from silicon. The results clearly show that higher tempering temperatures lead to a greater decrease in the normalized lattice parameter of retained austenite by the end of the holding stage. Since the lattice parameter is known to increase with carbon content, this trend indicates that retained austenite contains less carbon at higher tempering temperatures within the studied range. This observation is consistent with the measured variation in the martensite start (Ms) temperature as a function of tempering temperature.

IV. DISCUSSION

A. *Decomposition of Retained Austenite*

One of the most striking observations of this study concerns the sequence of decomposition of the retained austenite during tempering. In fact, it clearly appears from HEXRD measurements that most of the retained austenite remains untransformed during heating and holding time and transforms into fresh martensite during cooling. Thus, retained austenite during tempering follows the subsequent sequence of decomposition:

$$\gamma_{\text{retained}} \xrightarrow[\text{heat and tempering hold stage}]{} \gamma_{\text{retained}} + \text{M}_3\text{C carbides} \xrightarrow[\text{cooling}]{} \alpha' + \text{M}_3\text{C carbides} + \gamma_{\text{retained}}$$

It is widely accepted that the decomposition of retained austenite typically proceeds through transformation into ferrite and cementite, sometimes preceded

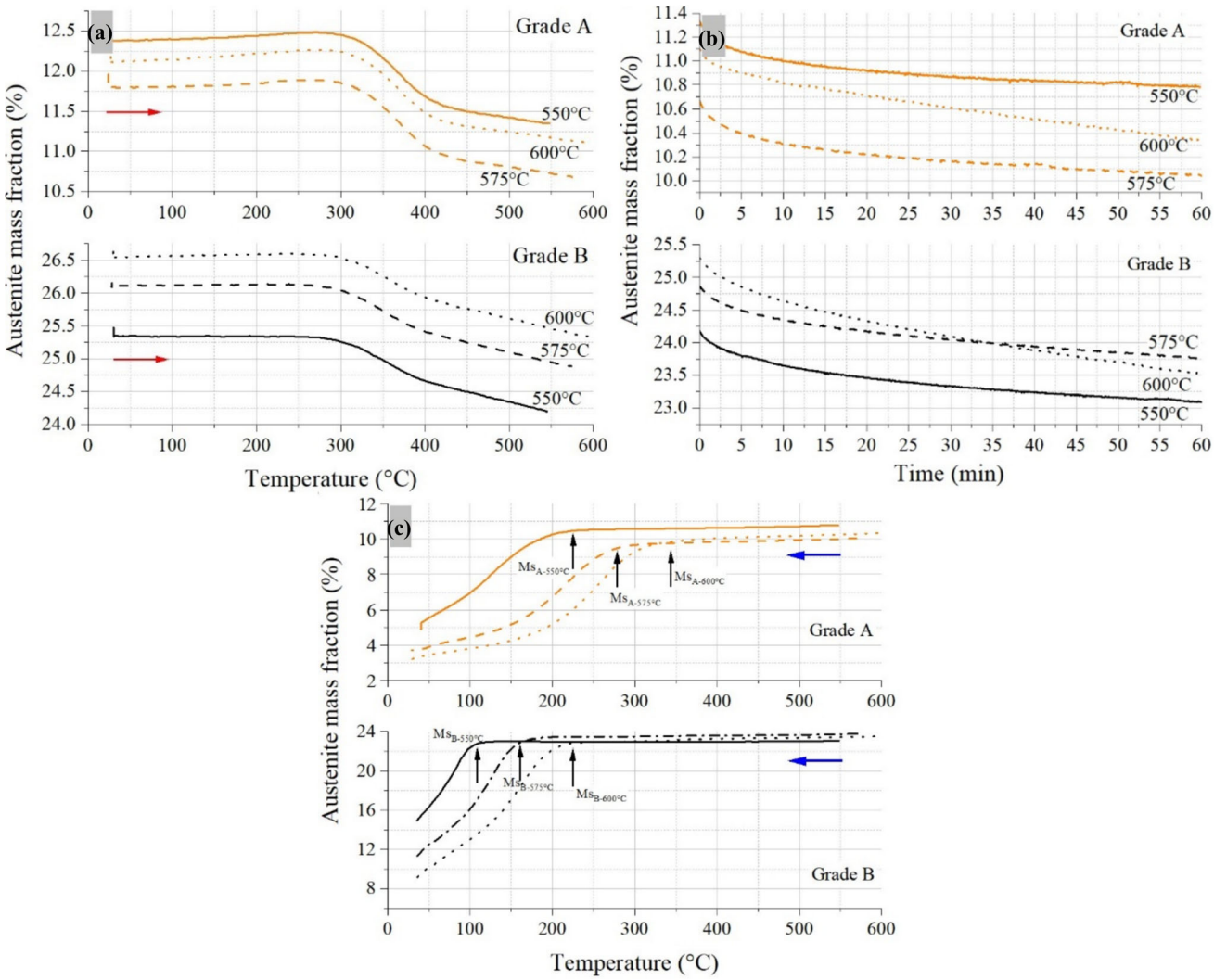

Fig. 9—Evolution of the retained austenite mass fraction during tempering process for both grades A and B; (*a*) during heating stage at 1 °C/s, (*b*) during tempering holding time for different tempering temperatures (550 °C, 575 °C, and 600 °C), (*c*) during cooling stage.

by the formation of transition carbides.[6] In certain cases, the transformation occurs via the formation of bainite.[7,8] In rare instances,[10,11] retained austenite has been shown to remain untransformed during tempering and to transform into martensite only during the subsequent cooling phase. This behavior was demonstrated in the cited studies through indirect methods, such as dilatometric analysis, and supported by TEM observations in.[10] In the present study, this transformation pathway is directly evidenced by HEXRD measurements. A common feature among studies reporting this decomposition sequence is the presence of an initial bainitic microstructure.

If considering rapid cooling from the austenitization, only little carbon partitioning is expected to occur between martensite and retained austenite resulting from the quenching. On the contrary, if the cooling is slower and allows the formation of a bainitic microstructure, in particular, a bainite containing a low amount of carbides, the austenite is expected to enrich in carbon during the bainitic transformation, leading to a more stable retained austenite. When tempering this type of retained austenite, it may be difficult to decompose. What is observed in the current study is the formation of carbides from the excess carbon in retained austenite but no further transformation of retained austenite into ferrite or bainite. As a consequence, retained austenite, still having a high content of carbon but lower than in the initial state, is prone to transform into fresh martensite during the cooling stage of the tempering.

The carbon content in retained austenite plays a key role in determining its stability. The lattice parameter measured by HEXRD can be used to estimate this carbon content.[39,40] Specifically, it can be derived from the experimental lattice parameter of retained austenite using the empirical formula [1] proposed by Dyson and Holmes[41]:

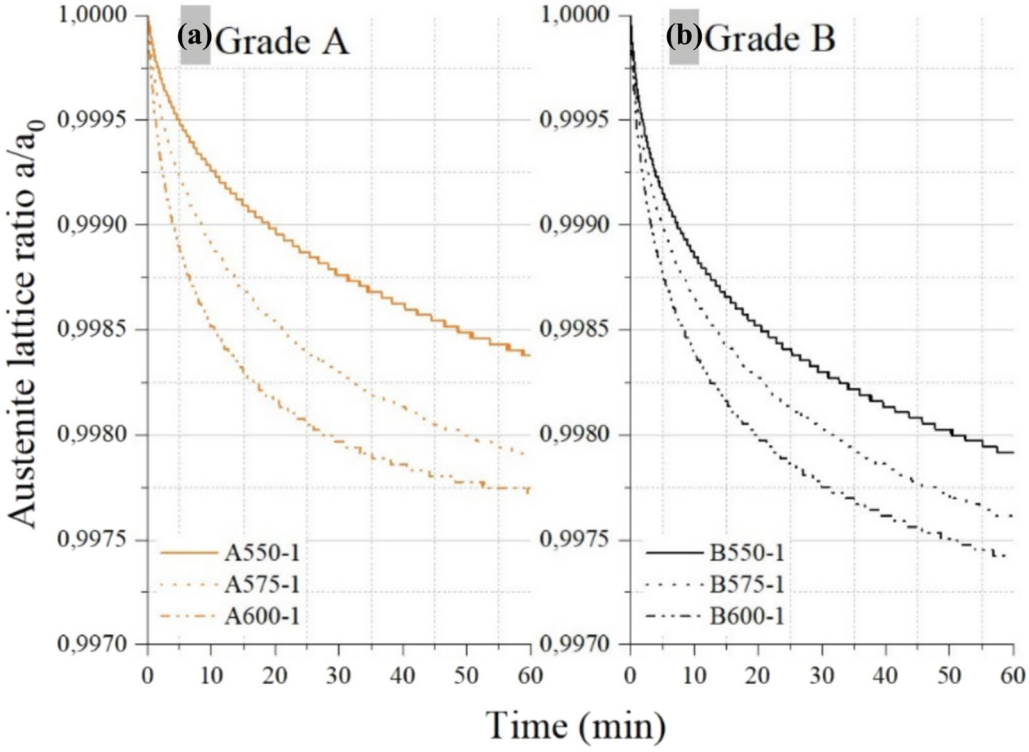

Fig. 10—Evolution of the retained austenite mean lattice parameter during tempering time normalized by the parameter at the beginning of the holding period for different tempering temperatures (550 °C, 575 °C, and 600 °C), with a heating rate of 1 °C/s (*a*) grade A (*b*) grade B.

$$a_\gamma = 3.5782 + 0.033w_c + 0.00095w_{Mn} - 0.0002w_{Ni} + 0.0006w_{Cr} + 0.0056w_{Al} + 0.0031w_{Mo} + 0.0018w_V, \quad [1]$$

where w_i is the weight fraction of the alloying element i in the austenite and $a\gamma$ is the lattice parameter in Å. It is assumed in the following that the substitutional alloying elements do not partition, and so w_i is taken equal to the nominal composition for $i \neq C$ (exact compositions from chemical analysis were considered in the calculations) and mechanical effect on the lattice parameter variation is also neglected. The estimation of carbon content in retained austenite gives 0.67 wt pct C for grade A and 0.83 wt pct C for grade B in the initial state (before tempering). As expected from previous considerations, retained austenite is enriched as compared to the nominal chemical composition of the steels (0.35 wt pct C). Notably, the retained austenite in grade B—present in a larger fraction (26 pct compared to 12 pct in grade A)—also exhibits a higher carbon content. This can be attributed to the higher silicon content in grade B, as silicon is known to inhibit cementite formation. This is consistent with the lower amount of cementite observed in the initial state (Figure 3b).

It is possible to evaluate the carbon content in the austenitic phase before martensitic transformation. However, as the lattice parameter is primarily affected by the thermal expansion, it is necessary to remove the thermal contribution. To this end, the variation in lattice parameter can be evaluated at the same temperature during both heating and cooling, ensuring that no transformation has yet occurred in retained austenite during heating, and that the martensite start (Ms) temperature is not reached during cooling. As depicted by the arrow drawn in figure 8-a, temperature 300 °C responds to these criteria for all samples, except the sample A-600 °C at 1 °C/s for which the M_s temperature is slightly higher. The variation in lattice parameter thus corresponds to the variation in carbon content in the retained austenite during tempering before its transformation into martensite. The values of carbon content in retained austenite before its martensitic transformation during cooling in grades A and B for the three tempering temperatures 550, 575 and 600 °C are reported in Table III for the heating rate of 1 °C/s.

From these calculations, it clearly appears that the higher the temperature of tempering, the lower the carbon content in the retained austenite at the end of tempering stage. As expected, the higher tempering temperature promotes a more abundant precipitation of carbides, leading to a higher depletion of retained austenite in carbon. Moreover, grade B, which contains more silicon, favors a higher overall carbon content in the retained austenite, as already discussed.

B. *Effect of Silicon*

The as-quenched retained austenite content differs significantly between grades A and B: Grade A contains approximately 12 pct by mass, while grade B reaches

Table III. Estimation of the C Content in Retained Austenite, Resulting Estimation for M_s Temperature, and Estimation Volume Fraction of Cementite from the Variation in Lattice Parameter of Retained Austenite for Both Grades Tempered at 550 °C, 575 °C, and 600 °C with a Heating Rate of 1 °C/s

	Estimated C Content in Retained Austenite (Wt Pct C)		Martensite Start Temperature M_S (°C)		Estimated Volume Fraction of M_3C (Pct)
	Initial state	Before M_S	Measured	Calculated from Eq. [2]	Final State
A-550 °C	$0.67^{\pm 0.01}$	$0.42^{\pm 0.01}$	$230^{\pm 5}$	$269^{\pm 5}$	$4.6^{\pm 0.1}$
A-575 °C		$0.34^{\pm 0.01}$	$300^{\pm 5}$	$307^{\pm 5}$	$4.7^{\pm 0.1}$
A-600 °C		$0.29^{\pm 0.01}$	$320^{\pm 5}$	$329^{\pm 5}$	$4.8^{\pm 0.1}$
B-550 °C	$0.83^{\pm 0.01}$	$0.60^{\pm 0.01}$	$130^{\pm 5}$	$178^{\pm 5}$	$3.2^{\pm 0.1}$
B-575 °C		$0.53^{\pm 0.01}$	$175^{\pm 5}$	$214^{\pm 5}$	$3.4^{\pm 0.1}$
B-600 °C		$0.46^{\pm 0.01}$	$220^{\pm 5}$	$244^{\pm 5}$	$3.6^{\pm 0.1}$

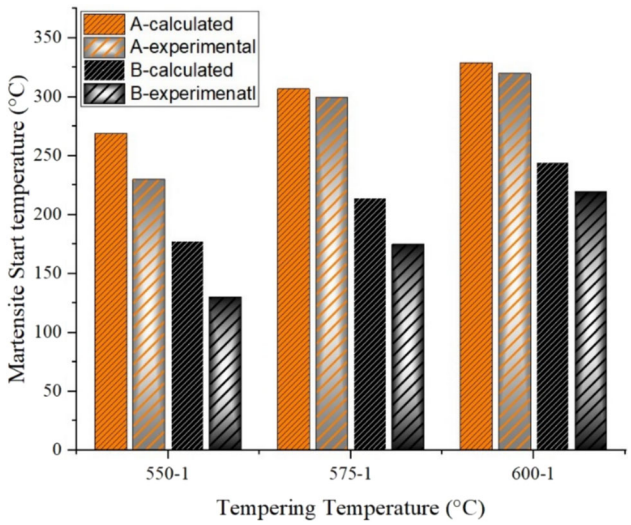

Fig. 11—Comparison of calculated martensite start temperature as a function to the tempering temperature and to experimental results measured by HEXRD for both grades.

nearly 26 pct. This difference is primarily attributed to the higher silicon content in grade B, which is about four times greater than in grade A. Silicon, a well-known non-carbide-forming element, has been extensively studied in recent literature, particularly regarding its role during tempering in low-carbon steels.[13,35,42,43] An increased silicon content is known to promote higher fractions of retained austenite in steel.[42] Furthermore, as already mentioned, the initial carbon content of retained austenite in grade B is significantly higher than the one in grade A.

The remarkable difference between grade A and grade B [see Figure 9(c)] arises from the variation in the M_S values, with a shift of around 100 °C between grade B and grade A, whatever the tempering temperature. This is attributed to a higher stability of the retained austenite due to silicon addition in grade B. This is confirmed by the estimation of the carbon content in the retained austenite before the martensite transformation, when comparing in Table III the two steels in the same conditions.

Considering that the M_S temperature is primarily determined by the carbon content in the retained austenite before transformation, it is possible to evaluate the M_S temperature by using empirical relationships. Many relationships relating M_S and the chemical composition are available in the literature.[44] Over all these relationships, the following equation (2) is the one that gives the best agreement with the experimental data:

$$M_s = 561 - 474 * w_c - 33 * w_{Mn} - 17 * w_{Cr} - 17 * w_{Ni} - 21 * w_{Mo} + 10 * w_{Co} - 7.5 * w_{Si} \quad [2]$$

where the contents of carbon, manganese, chromium, nickel, molybdenum, cobalt, and silicon are in wt pct. In the calculation, carbon content in retained austenite is the value calculated before martensite transformation, as reported in Table III. For other elements, the nominal composition was considered.

The M_s temperatures calculated from equation (2) are displayed in Table III and plotted as a function of tempering temperature for both grades in Figure 11. The experimental M_S data are extracted from variation in the retained austenite amount [see Figure 8(c)]. In spite of an overall overestimation of the calculated M_S temperature, it highlights an unambiguous difference between grades: The B grade has lower M_s compared to grade A. This is in line with literature as the silicon element is expected to affect the retained austenite decomposition in two ways:

- The capacity to promote the carbon distribution from martensitic or bainitic phases to the austenite leads to longer stability of the austenite and limits its decomposition.[35] Thus, the martensitic transformation is postponed in rich silicon alloy.
- Silicon alloying element affects also the kinetics of carbide precipitation during the tempering process; it is reported that it restricts the diffusion of carbon and affects mainly the nucleation and the growth of cementite carbides.[35] This is also in agreement with the HEXRD results as limited cementite carbides were identified comparatively to grade A (see paragraph 3.2).

C. *Effect of the Heating Rate*

Our results show that the behavior of the retained austenite during tempering is slightly affected by the heating rate. The main effect is the occurrence of a slight decrease in retained austenite fraction at a temperature between 300 °C and 400 °C in the case of slow heating rate [see Figure 9(a)] that is not observed in the high heating rate experiment. This transformation can be attributed to the precipitation of fine particles of ε-carbides with a composition close to $Fe_{2.4}C$, which should dissolve to give rise to the more stable cementite phase. However, due to their low fraction and their nanometric size leading to strong line broadening, it was not possible to detect the ε-carbides.

D. *Effect of the Tempering Temperature*

As stated before, increasing the tempering temperature should increase the amount of carbides formed. HEXRD allows the determination of the precipitated carbide content in two ways: either the quantification using the Rietveld procedure considering the peaks of α, γ phases and Fe_3C carbide (method 1) or the mass balance of carbon considering the same phases (method 2).

The mass fraction calculated through the Rietveld refinement (method 1) of the A and B grades at the initial state was found to be 1 pct and lower than 1 pct, respectively. After tempering process, the mass fraction increases in both grades, reaching 3 pct for the grade A and 1 pct for the grade B, whatever the considered tempering temperature.

Using equation (1), the final carbon content in retained austenite is deduced and used to estimate the weight fraction of carbides (method 2). Equation (3) is the mass balance used for this calculation:

$$w_{C0} = w_\alpha * f_\alpha + w_\gamma * f_\gamma + w_C * f_C \qquad [3]$$

where w_{C0} is the nominal carbon content in the alloy, w_i is the weight fraction of carbon in the different phases, *and* f_i is the weight fraction of phase i in the system. By assuming that the ferrite α contains no carbon and the carbide has 6.67 pct wt of carbon, the weight fraction of cementite can be estimated.

In the initial state, the calculation gives about 4 wt pct cementite for the grade A and 2 wt pct for the grade B. These values are higher than those measured by HEXRD in the initial state, probably because of the presence of small carbides that cannot be correctly accounted for in method 1. The estimated weight fractions of carbide after tempering at the various temperatures in both grades are given in Table III. These results confirm also the role of silicon on limiting the precipitation of cementite carbide.

V. CONCLUSION

Based on all the results obtained in this study, and using a combined analysis of the phase mass fractions and their mean lattice parameters from *in situ* synchrotron HEXRD, complemented by microscopic observations, the following conclusions can be drawn for the two low-carbon steel grades A and B, which differ only in their silicon content and underwent comparable tempering treatments:

- The *in situ* experiment allows to clearly demonstrate that, in all studied conditions, retained austenite mainly transforms by the so-called indirect transformation, *i.e.,* during the cooling stage of the tempering process and forms fresh martensite.
- The retained austenite decomposition starts early during the heating stage with slow heating rates leading to the development of carbides, which are absent in the fast heated samples at the end of heating.
- The addition of the silicon alloying element affects the amount of retained austenite in the initial state as well as cementite kinetics during tempering. The *in situ* HEXRD obtained with grade B for slow heating rate proves their postponed precipitation process.
- The amount of retained austenite decreases after tempering, while the remaining austenite becomes more stable. This stability depends on the tempering temperature and is linked to changes in the chemical composition of retained austenite prior to cooling.

ACKNOWLEDGMENTS

The authors would like to thank DESY at the P07 beamline in Hamburg (Germany) for the provision of experimental facilities (proposal I-20211094 EC). We are grateful to C. Almeida Da Fonseca, J. Audard, P. Barges, and D. Obriot for their help in the microscopic observations.

CONFLICT OF INTEREST

The authors declare that they have no conflict of interest.

FUNDING

Open access funding provided by Arts et Metiers Institute of Technology.

REFERENCES

1. R.A. Mesquita, Tool Steels: Properties and Performance, Boca Raton, ISBN 9780367782573, 2016. https://doi.org/10.1201/9781315181516.
2. J.Y. Son, K.Y. Lee, G.Y. Shin, C.H. Choi, and D.S. Shim: *Micromachines.*, 2023, https://doi.org/10.3390/mi14040872.
3. S.H. Talebi, M. Jahazi, and H. Melkonyan: *Materials (Basel).*, 2018, vol. 11, p. 1441.
4. S.M. Chentouf, M. Jahazi, L.-P. Lapierre-Boire, and S. Godin: *Metallogr. Microstruct. Anal.*, 2014, vol. 3, pp. 281–97.
5. C. Lerchbacher, S. Zinner, and H. Leitner: *Mater. Sci. Eng. A*, 2013, vol. 564, pp. 163–68.
6. C. Lerchbacher, S. Zinner, and H. Leitner: *Met. Mater. Trans. A*, 2012, vol. 43A, pp. 4989–98.
7. G. Yan, L. Han, C. Li, X. Luo, and J. Gu: *J. Nucl. Mater.*, 2017, vol. 483, pp. 167–75.
8. S. Hesamodin Talebi, H. Ghasemi-Nanesa, M. Jahazi, and H. Melkonyan: *Metals (Basel)*, 2017, vol. 7, p. 346.
9. Z. Jiang, P. Wang, D. Li, and Y. Li: *Mater. Sci. Eng. A*, 2019, vol. 742, pp. 540–52.
10. A. Saha Podder and H.K.D.H. Bhadeshia: *Mater. Sci. Eng. A.*, 2010, vol. 527, pp. 2121–28.
11. C. Lerchbacher, The Effect of Cooling Rate on the Microstructure and its Influence on Toughness of two Types of Tool Steels Studied by High Resolution Techniques, Doctoral thesis, 2013.
12. A. Rehan, A. Medvedeva, L.E. Svensson, and L. Karlsson: *Metall. Mater. Trans. A*, 2017, vol. 48A, p. 5233.
13. V.K. Euser, D.L. Williamson, A.J. Clarke, and J.G. Speer: *ISIJ Int.*, 2020, vol. 60, pp. 2990–3000.
14. S.H. Talebi, H. Ghasemi-Nanesa, M. Jahazi, and H. Melkonyan: *Metals*, 2017, vol. 7, p. 346.
15. T. Sourmail, L. Otter, S. Collin, M. Billet, A. Philippot, F. Cristofari, and P. Secordel: *Mater. Charact.*, 2021, vol. 173, p. 110922.
16. P. Kirbiš, I. Anžel, and M. Brunčko: *Phys. Met. Metallogr.*, 2016, vol. 117, pp. 1130–39.
17. M. Villa, F. Niessen, and M.A.J. Somers: *Metall. Mater. Trans. A*, 2018, vol. 49A, pp. 28–40.
18. B. Kim, E. Boucard, T. Sourmail, D. San Martin, N. Gey, and P.E.J. Rivera-Diaz-del-Castillo: *Acta Mater.*, 2014, vol. 68, pp. 169–78.
19. D.H. Sherman, S.M. Cross, S. Kim, F. Grandjean, G.J. Long, and M.K. Miller: *Metall. Mater. Trans. A*, 2007, vol. 38A, pp. 1698–1711.
20. G.G. Ribamar, G. Miyamoto, T. Furuhara, J.D. Escobar, J.A.A. Vila, E. Maawad, N. Schell, J.P. Oliveira, and H. Goldenstein: *Metall. Mater. Trans. A.*, 2024, vol. 55A, pp. 93–100.
21. S.Y.P. Allain, S. Gaudez, G. Geandier, J.-C. Hell, M. Gouné, F. Danoix, M. Soler, S. Aoued, and A. Poulon-Quintin: *Mater. Sci. Eng. A*, 2018, vol. 710, pp. 245–50.
22. D. Foster, M. Paladugu, J. Hughes, M. Kapousidou, U. Islam, A. Stark, N. Schell, and E. Jimenez-Melero: *Mater. Today Commun.*, 2021, vol. 29, p. 102930.
23. S. Gaudez, J. Teixeira, S. Denis, G. Geandier, and S.Y.P. Allain: *Mater. Charact.*, 2022, vol. 185, p. 111740.
24. S.Y.P. Allain, S. Gaudez, G. Geandier, F. Danoix, M. Soler, and M. Goune: *Scr. Mater.*, 2020, vol. 181, pp. 108–14.
25. N. Hosseini, F. Forouzan, and E. Vuorinen: *Mater. Today Commun.*, 2022, vol. 31, p. 103503.
26. B. Denand, V.A. Esin, M. Dehmas, G. Geandier, S. Denis, T. Sourmail, and E. Aeby-Gautier: *Materialia*, 2020, vol. 10, p. 100664.
27. A.P. Hammersley, FIT2D: An Introduction and Overview, ESRF Internal Report, ESRF97HA02T, 1997.
28. J. Rodriguez-Carvajal: *Physica B*, 1993, vol. 192, pp. 55–69.
29. E.F. Rauch and M. Véron: *Mater. Charact.*, 2014, vol. 98, pp. 1–9.
30. J.D. Verhoeven, A.H. Pendray, and E.D. Gibson: *Mater. Charact.*, 1996, vol. 37, pp. 9–22.
31. J. Dong, X. Zhou, Y. Liu, C. Li, C. Liu, and Q. Guo: *Mater. Sci. Eng. A*, 2017, vol. 683, pp. 215–26.
32. T. Zhou, R.P. Babu, Z. Hou, J. Odqvist, and P. Hedström: *Materialia*, 2020, vol. 9, p. 100630.
33. E. Claesson, H. Magnusson, and P. Hedström: *Mater. Charact.*, 2023, vol. 202, p. 113032.
34. K. Zhu: *J. Mater. Sci.*, 2018, vol. 53, pp. 6951–67.
35. L. Li, Z. Cai, and X. Wu: *Metals*, 2023, vol. 13(1), p. 100.
36. V.K. Euser, D.L. Williamson, K.O. Findley, A.J. Clarke, and J.G. Speer: *Metals (Basel)*, 2021, vol. 11, p. 1349.
37. L. Morsdorf, A. Kashiwar, C. Kübel, and C.C. Tasan: *Mater. Sci. Eng. A*, 2023, vol. 862, p. 144369.
38. F.G. Caballero, H.W. Yen, M.K. Miller, J. Cornide, H.T. Chang, C. Garcia-Mateo, and J.R. Yang: *Mater. Charact.*, 2014, vol. 88, pp. 15–20.
39. N.H. van Dijk, A.M. Butt, L. Zhao, J. Sietsma, S.E. Offerman, J.P. Wright, and S. van der Zwaag: *Acta Mater.*, 2005, vol. 53, pp. 5439–47.
40. C.P. Scott and J. Drillet: *Scr. Mater.*, 2007, vol. 56, pp. 489–92.
41. D.J. Dyson and B. Holmes: *J. Iron Steel Inst.*, 1970, vol. 208, pp. 469–74.
42. B. Kim, J. Sietsma, and M.J. Santofimia: *Mater. Des.*, 2017, vol. 127, pp. 336–45.
43. A. Varshney, K. Mondal, and S. Sangal: *Mater. Sci. Eng. A*, 2022, vol. 832, p. 142455.
44. J. Platl, H. Leitner, C. Turk, and R. Schnitzer: *Steel Res. Int.*, 2020, vol. 91, pp. 1–8.